Z. Geomorph. N.F.	52	Suppl. 2	35 – 55	Berlin · Stuttgart	September 2008

Holocene morphodynamics in the Ugii Nuur basin, Mongolia – insights from a sediment profile and 1D electrical resistivity tomography

Wolfgang Schwanghart und Brigitta Schütt

with 7 figures and 1 table

Summary. Sediment profile analysis and electrical resistivity tomography were applied in the Ugii Nuur basin, central Mongolia, in order to gain insight into the sedimentary architecture of valley fillings. It is shown that important constituents in the near surface ground are aeolian fines. Coarse grainsizes were predominantly deposited during the Late Pleistocene and the beginning of the Holocene indicating local dune activity and arid conditions. Since the Early to Mid Holocene a larger proportion of silt suggests an increase in mineral dust deposition. In combination with soil formation this points at dust trapping by a denser vegetation cover that reflects more humid conditions in the Ugii Nuur basin. Yet, 1D electrical resistivity tomography (VES) shows that Holocene deposits represent only a minor part of the thick valley fillings. Hence, it is assumed that their main extent has been established during the Pleistocene.

Keywords. aeolian deposits, hill wash deposits, calcrete, soil sediments

1 *Introduction*

The Ugii Nuur basin is an ideal location to study Holocene landscape development and climate evolution in the highly continental area of the steppe region of Mongolia. Distinct features of this area are thick layers of debris accumulated and reworked by periglacial, aeolian, fluvial or hill wash processes. The vastness of these debris covers can be especially recognized from air photographs where their extent leaves a mark of a landscape drowning in its own sediments.

The processes generating these debris covers and the temporal placement of their genesis are poorly understood. In this study we investigated the sedimentary architecture of valley fillings by 1D vertical electrical sounding (VES) and a profile description in order to understand the depositional processes and environments in the Ugii Nuur basin. Electrical resistivity tomography is a valuable tool in geomorphological surveys as it provides insight into the structure of the near surface ground (Dahlin 2001, Kneisel 2003, Löwner et al. 2005). Most prominently it has been applied in permafrost research – a discipline where electrical soundings benefit from the strong contrast in electrical conductivity between ground ice and overlying debris (Hauck & Vonder Mühll 2003, Kneisel 2004, 2005, Krautblatter & Hauck 2007). Other fields of application are predominantly geoarcheological investigations where buried remnants of walls could be detected in several meters depth (Piro et al. 2000, Aspinall & Gaffney, 2001). Our investigation aims at the application of this geophysical tool to quantify thickness of valley fillings. The overall goal of the presented work is to contribute to the understanding of the Holocene climate and landscape evolution of today's steppe region of Mongolia.

DOI: 10.1127/0372-8854/2008/0052S2-0035 0372-8854/08/5202-0035 $ 5.25
© 2008 Gebrüder Borntraeger, D-14129 Berlin · D-70176 Stuttgart

2 *State of the Art*

The origin of the vast debris cover accumulations has been previously explained by several authors for different areas (Berkey & Morris 1927, Richter et al. 1963, Haase 1983, Walther & Naumann 1997, Grunert et al. 2000, Lehmkuhl & Haselein 2000, Jadambaa et al. 2003). Grunert et al. (2000) and Lehmkuhl & Haselein (2000) describe the thick deposits of unconsolidated debris and fluvial sediments in the Uvs Nuur basin as interfingering alluvial fans and fanglomerates, and describe them as pediments (bajadas). They assume that their formation predominantly occurred during the cold periods of the Pleistocene. Owen et al. (1997) and Owen et al. (1998) investigated vast alluvial fans prograding from the mountain ranges in the Gobi desert in southern Mongolia. They affiliate their predominant formation to hill wash and fluvial processes during the period from 23–9 ky BP, when the climate was more arid, flash flooding dominated and ephemeral streams deposited coarse fanglomerates.

According to Lehmkuhl & Lang (2001) enhanced moisture supply and subsequent denser vegetation cover led to a general reduction in sediment yield during the Early Holocene. Increased moisture availability is recorded in various archives like lake sediments by a rapid increase in lake levels (Walther et al. 2003), which is likely linked to the abrupt monsoon intensification at ~11.5 ky BP (Sirocko et al. 1993, Wang et al. 1999, Herzschuh 2006). Rising lake levels, however, may partly be explained by increased melt water supply from glaciated areas due to increased net summer insolation (Walther 1999, Walther et al. 2003). According to Gunin et al. (1999) steppe vegetation dominated at most sites in Mongolia and deserts occupied large depressions in western Mongolia from 11.5 to 8.9 ky BP. Partly, this aridisation resulted in a decrease in lake levels (Walther et al. 2003) and reactivation of dune fields (Grunert et al. 2000).

Mid Holocene (8.9–4.5 ky BP) records provide an ambivalent picture of Mongolia's climate during this time. While many areas experienced better moisture conditions (Gunin et al. 1999, Tarasov et al. 2000, Grunert & Dasch 2004, Yang et al. 2004) with minor fluctuations (Walther et al. 2003), significant forest covers cannot be recognized in most pollen profiles (Gunin et al. 1999, Rösch et al. 2005). Moreover, records of Lake Hovsgol and Baikal (Prokopenko et al. 2007), Lake Telmen (Peck et al. 2002, Fowell et al. 2003) and GCM simulations (Bush 2005) suggest a trend towards dryer conditions during the Mid Holocene. A prevalence of moisture conditions similar to present since ~4 ky BP (Gunin et al. 1999, Prokopenko et al. 2007) is locally interrupted by short dryer and wetter periods (Peck et al. 2002, Fowell et al. 2003, Walther et al. 2003).

At present, ephemeral streams trench the extended debris covers and deposit much smaller fans than those deposited during Pleistocene glacial periods due to a reduction in sediment supply and increased vegetation cover (Lehmkuhl & Haselein 2000, Lehmkuhl & Lang 2001). An important constituent in the debris covers is a high content of silt and fine sands whose origin, on the one hand, is regarded as product of intensified weathering during the glacial stages. On the other hand it has been shown that a horizontal cycle of mobilization of silts and sands deposited in ancient river courses and lake systems, short to long range transport and consecutive deposition by the wind led to a redistribution of these fines during the interstadials (Grunert et al. 2000,

Grunert & Lehmkuhl 2004). Yet, the importance of aeolian processes in the generation of loess like deposits and dune fields is high as investigations on current wind blown dust suggest (Natsagdorj et al. 2003, Dulam 2005).

3 *Study site*

Ugii Nuur is a quasi-endorheic lake located at 47°44'N and 102°46'E at an elevation of 1328 m (EGM96) (Figs. 1 and 2). The lake is situated at the eastern flank of the Middle Orkhon Valley, which runs in northward direction and is formed by the Orkhon Gol (Orkhon River) in the west and Chögschin Orkhon Gol (Old Orkhon River) in the east. At present, the lake is fed by the Old Orkhon River and episodically drains into the Orkhon River during high lake levels.

The climate of the area is extremely continental and can be described as BSk-climate following the classification concept of Köppen (Kottek et al. 2006). Mean annual air temperature is around 0°C and annual precipitation sums up to 250 mm. A strong seasonality marked by extremely high annual temperature amplitude and a pronounced contrast between winter and summer precipitation amounts reflect the varying influence of air masses and insolation. While snow depths of 10 cm are hardly exceeded during the winter months, precipitation during July amounts up to 180 mm and often constitutes in storm events (Barthel 1983).

Lake Ugii Nuur is located along a graben structure. Tertiary volcanism east of the Ugii Nuur basin points to increased Cenozoic tectonic activity (Walther & Gegeensuvd 2005). The bedrock mainly consists of Carboniferous, highly fissile mudstones that dip almost perpendicular (Traynor & Sladen 1995, Sladen & Traynor 2000, Jadambaa et al. 2003). Cliff lines along Ugii Nuur's southern shoreline expose reddish late Cretacious and Tertiary conglomerates that provide evidence for fluvial dynamics with high bedload transport as documented by pebble beds and channel bar sandstones (Traynor & Sladen 1995).

Relief differs between the northern and southern part of the basin (Fig. 2). The north is characterized by hilly to mountainous terrain with elevations up to 1600 m while the south has a gentle undulating relief with broad saucer-shaped valleys. Both in the northern and southern part of the basin, valleys are filled with thick debris covers reflecting the interfingering influence of slope processes as frost weathering and cryoturbation, solifluction and accumulation of material displaced by hill wash, fluvial accumulation along the channels and wind-driven deposition of a loess-like sediment coverage.

The Ugii Nuur basin is located within the zone of highly continental steppe soil formation (Opp & Hilbig 2003). Soils found in the Ugii Nuur basin predominantly consist of Kastanozems (Haase 1983) while Regosols and Leptosols dominate on steep slopes and ridges. Soils are loamy to sandy riddled with a considerable amount of debris and pebbles that are often layered and adjusted. The study site is situated within the area of dry, gras steppes (Hilbig 1995, Opp & Hilbig 2003) and is dominated by grasses (*Cleistogenes, Stipa*), forbs (*Allium*), and shrubs (*Artemisia, Caragana*) while trees lack throughout the study site.

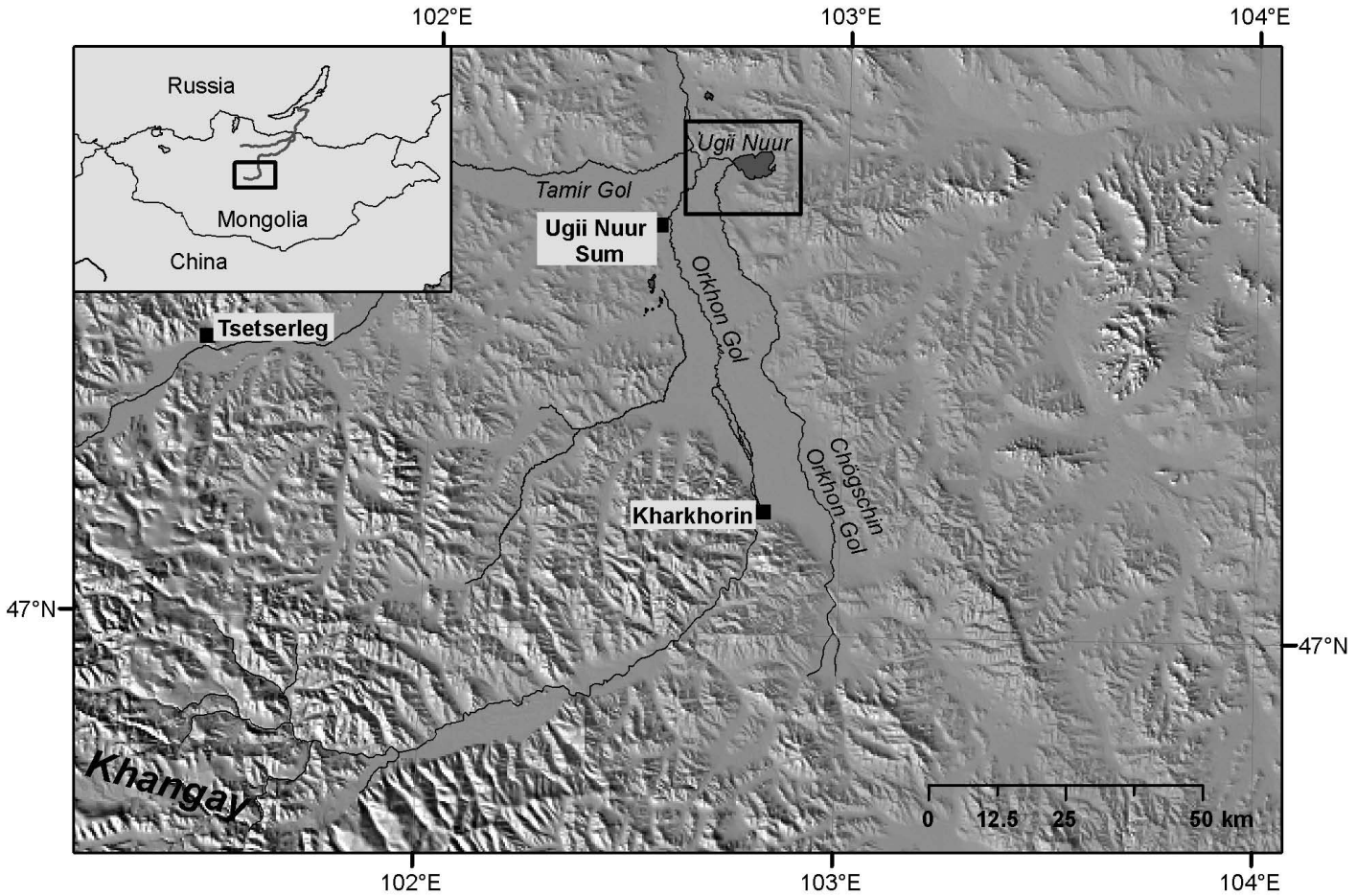

Fig. 1. Location of the study area. Hillshading is based on SRTM-3 data.

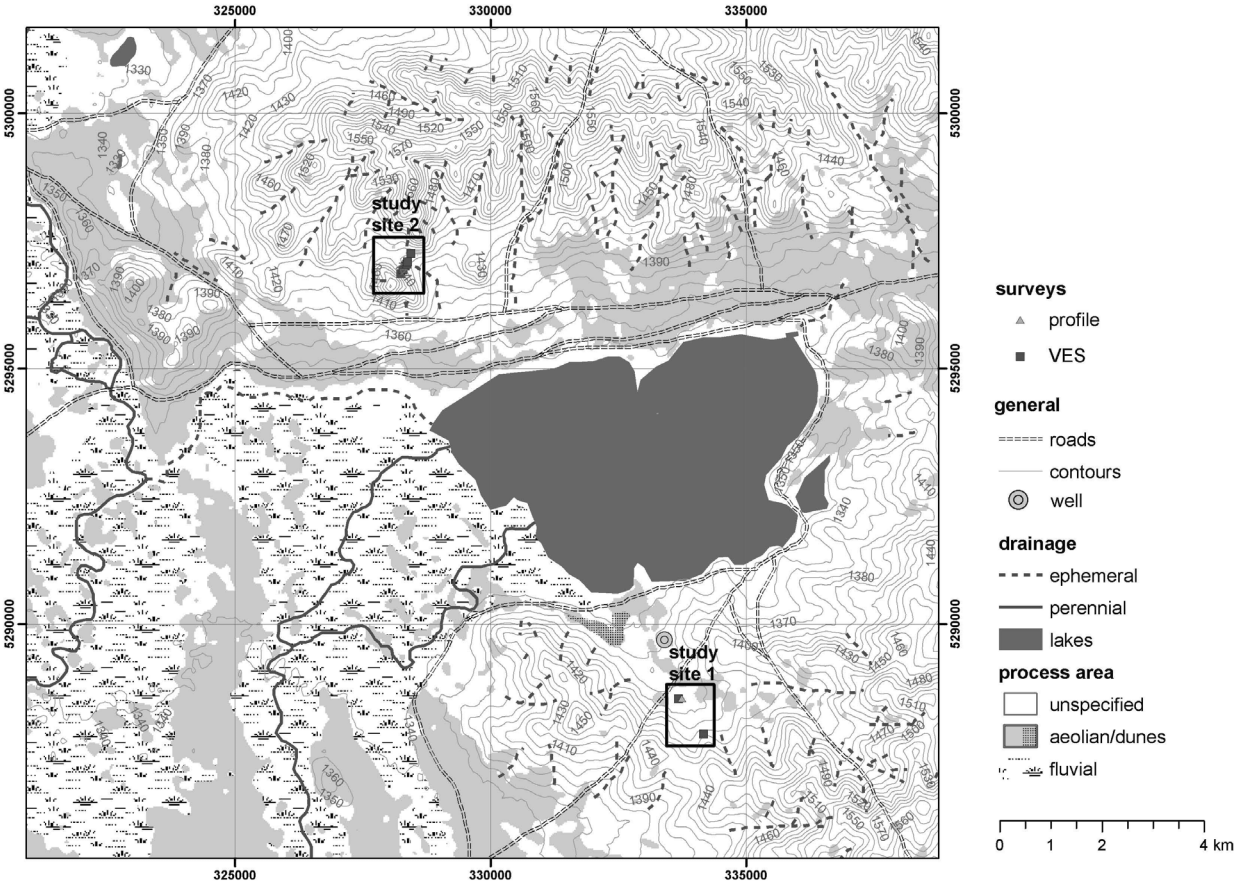

Fig. 2. Map of the Ugii Nuur basin with locations of the study sites.

4 *Methods*

Vertical electrical soundings (VES) were performed using an Oyo McOhm Model 2115A Mark-2. The Schlummberger array geometry with a four electrode configuration was chosen as it is less affected by lateral variations in layer thickness and resistivity (Kneisel 2003). Current (C) electrode spacings s [m] were increased exponentially by $s(i)/2=10^{i/8}$ m with i=1,2,... as index of electrode placing. The distance a of the potential (P) electrodes was set to a/2=0.5 m with s/2<17 m. At larger C electrode spacings the P electrode spacing was increased to a/2=1.5 m. The apparent resistivity [Ωm] is the product of the measured resistivity R [Ω] and the geometry factor K (Mussett & Khan 2000). K was calculated by

$$K = \frac{\pi}{a}\left(\left(\frac{s}{2}\right)^2 - \left(\frac{a}{2}\right)^2\right) \quad (1)$$

Modeling of vertical apparent resistivity profiles and of inverted layer models (Dahlin 2001) was performed using the interpretation software ResixIp (Interpex LTD).

A Differential Global Positioning System (DGPS) performing code correction was used to survey landforms. The DGPS was a combination of two Ashtech Mobilemapper Pro™ as rovers and an Ashtech Promark™ as reference station. The software Mobilemapper Office™ was applied to postprocess the data. The DGPS enables the kinematic recording of point, line and area features with submeter accuracy.

Soil profile descriptions were carried out according to the guidelines of AG Bodenkunde (2005), yet, when referring to soil type we refer to the World Reference Base (WRB) system. Samples were taken in 10 cm intervals and age control was gained by three radiocarbon datings conjointly on humins and humic acids by the Poznan Radiocarbon Laboratory. Calibration of radiocarbon dates was accomplished with CalPal, a software for calibration and visualization developed and distributed by the Prehistory Institute at University Cologne. As calibration curve CalPal2004-SFCP was used.

Sample preparation included drying at 50°C in a drying cabinet and subsequent homogenisation in an agate swing-sledge mill. Prior to chemical analysis sample material was screened and components larger 2 mm were rejected. Total organic carbon (TOC) and inorganic carbon (TIC) content were measured with a carmhograph (Wösthoff) (detection limit = 0.02 weight-% C), organic carbon content was calculated as the difference of both values. Element analysis was performed by inductively coupled plasma atomic emission spectroscopy (ICP-AES, Optima 3000, Perkin Elmer) of the Aqua Regina extracted samples. Loss of ignition was determined at 550°C for the air dried, not homogenized sample.

The mineralogical composition was specified by X-ray powder diffraction analyses using a copper kα-tube from 2–52 °2θ with steps of 0.01 °2θ and each step measured for one minute. Contents of mineral components were recorded semi-quantitativly by the diffraction-intensity at the mineral's major diffraction peak (cps) relatively to the intensity of quartz at its major diffraction peak (d101) from counts per second (cps) whereas 50 cps refers to spurs, 50–200 cps to low, 200–500 cps to low-medium, 500–1000 to medium, 1000–2500 cps to high and >2500 cps to very high content.

5 *Results*

5.1 *Study site 1*

The first site investigated is located in the southern part of the Ugii Nuur basin in a ca. 3 km broad, saucer-shaped valley running in northwest direction (Fig. 2). The relief is gently undulating to almost flat with an absence of forms indicating concentrated surface run-off.

Information on the character of valley sediments were derived from a profile of 250 cm depth (Fig. 3) dug on the south exposed slope in ca. 100 m distance from the depth contour of the valley. The profile's lithology can be subdivided into several distinct layers that have a very high fraction of fine sands in common as indicated by the dominance of quartz and feldspars by XRD (Table 1). Mica and amphiboles constitute only minor components of the mineral arrangement in the profile (Table 1). Soil is classified as Kastanozem with a litter cover of 40–50% and strong rooting to a depth of ca. 45 cm. Root-remnants are partially found down to a depth of 90 cm. The grain size composition in the upper 45 cm of the outcrop can be characterized by the scattered occurrence of fine gravel in a silty to sandy matrix (layers 1, 0–12 cm depth, and 2, 12–45 cm, Fig. 3).

Beneath 45 cm sediments change in color from light brown (layer 2, 12–45 cm) to brown (layer 3, 45–90 cm) and to light grey (layer 4, 90–115 cm). Grain size composition changes from fine sand and silt in layers 3 to fine sands in layer 4 and shows a slight trend with depth toward fine and middle sand. Next to this, layer 3 is characterized by increased TOC content that rapidly decreases in layer 4. The transition from layer 3 to 4 is very sharp. From 90–135 cm highly compacted, fine sands prevail, cemented by carbonate (layer 4 and 5) as indicated by reaction when treated with hydrochloric acid. Below layer 5 (115–135 cm), a diffuse transition into a less compacted, 10 cm thick, yellowish brown layer of carbonate free fine sands (layer 6, 135–145 cm) occurs. Beneath, a strangled layer, weakly humous and with carbonatic inclusions shows a brownish color (layer 7, 145–208 cm). This layer is underlain by light brownish fine sand with singular ferric oxide patches in the upper part (layer 8, 208–223 cm, and 9, 223–235 cm). Beneath 235 cm depth sediments are composed of pure fine to middle sand and exhibit a grayish color in layer 10 (235–240 cm) descending into a yellowish color in layer 11 in beneath a depth of 240 cm.

TIC contents along the whole profile are altogether low. Only in layers 4 and 5 TIC peaks at 0.4–0.55 mass-%. Carbonate contents in these layers are calculated to range between 2.4–4.4 mass-% and prevail as calcium carbonate (calcite) as indicated by XRD (Table 1). While carbonates occur as unlaminated and cemented in layers 4 and 5, they prevail as sparsely scattered concretions in the layers beneath. The depth functions of calcium concentrations show a similar pattern as the TIC throughout the profile.

TOC decreases from top to bottom. At the top TOC totals 1.6 mass-% and decreases in layer 2 to 0.8 mass-%. In layer 3 TOC concentrations show a slight increase to 1.2 mass-%, while in layer 4 TIC concentrations decline again with short term variations. In layer 5 TOC contents increase again and amount 0.5 mass-%. Except for a minor increase at the profile bottom, TOC ranges around 0.1 mass-% below layer 5. A Pearson correlation coefficient of 0.88 indicates a very good correlation of TOC and loss of ignition.

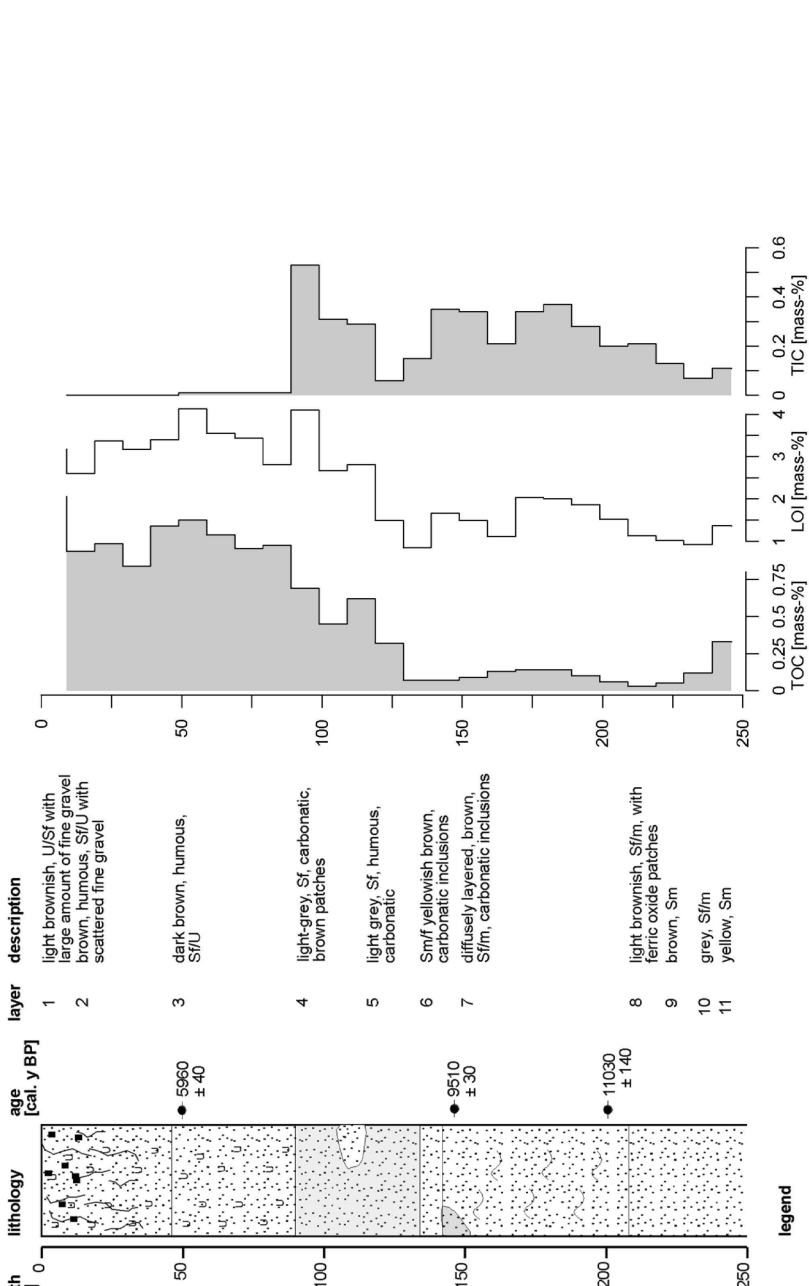

Fig. 3. Profile description in study site 1 and total inorganic carbon (TIC), total organic carbon (TOC) and loss of ignition (LOI) (see location of the profile in Fig. 2).

Table 1. Loss of ignition (LOI), carbonate content and mineral composition of samples taken in the sediment profile in study site 1.

depth [cm]	LOI [%]	carbonate content [%]	minerals [1] quartz	feldspars	amphibole	mica	calcite
9	3.18	0.00	+++++	+++	(+)	(+)	(+)
19	2.6	0.00	+++++	+++	(+)	(+)	(+)
29	3.37	0.00	++++	+++	(+)	(+)	(+)
39	3.17	0.00	++++(+)	+++	(+)	(+)	(+)
49	3.4	0.00	++++(+)	+++	(+)	(+)	(+)
59	4.13	0.08	++++(+)	+++	(+)	(+)	(+)
69	3.55	0.08	++++	+++	(+)	(+)	(+)
79	3.44	0.08	++++	+++	(+)	(+)	(+)
89	2.81	0.08	++++	+++	(+)	(+)	(+)
99	4.1	4.41	++++	+++	(+)	(+)	+
109	2.67	2.58	++++	++++	(+)	(+)	+
119	2.81	2.42	++++	+++	(+)	+	+
129	1.49	0.50	+++++	+++	(+)	(+)	(+)
139	0.85	1.25	+++++	+++	(+)	(+)	(+)
149	1.66	2.92	+++++	+++	(+)	(+)	(+)
159	1.49	2.83	+++++	+++	(+)	(+)	(+)
169	1.11	1.75	+++++	+++	(+)	(+)	(+)
179	2.03	2.83	+++++	+++(+)	(+)	(+)	(+)
189	2	3.08	++++(+)	+++(+)	(+)	(+)	+
199	1.86	2.33	++++(+)	++++	(+)	(+)	(+)
209	1.52	1.67	+++++	+++(+)	+	(+)	(+)
219	1.13	1.75	+++++	+++(+)	(+)	(+)	(+)
229	1.02	1.08	+++++	+++(+)	(+)	(+)	(+)
239	0.92	0.58	+++++	++++	(+)	(+)	+
246	1.37	0.92	+++++	++++	(+)	(+)	+

carbonate content (mass-%) = 8.33 x TIC (mass-%)

[1] estimation of quantity

(+)	traces	+++	medium
+	low	++++	high
++	low-medium	+++++	very high

The element composition varies along the profile (Fig. 4). Ca and S feature peaks are associated with the aforementioned carbonatic layers 4 and 5. Metals, heavy metals and PO show higher values in the upper part of the core before they tend to decline downward from the uppermost 20 cm. Their concentrations and TOC concentrations are positively correlated (e.g. $r_{TOC,Fe}$, $\alpha<0.01$, $n=21$).

A chronological framework of the profile was established by dating three samples in 50, 148 and 198 cm depth (Fig. 3). C ages constitute 4010±30, 8500±50 and 9670±50 uncal. years, respectively. Calibration against independent estimates of calendar ages yields 5960±40, 9510±30 and 11030±140 cal. years BP.

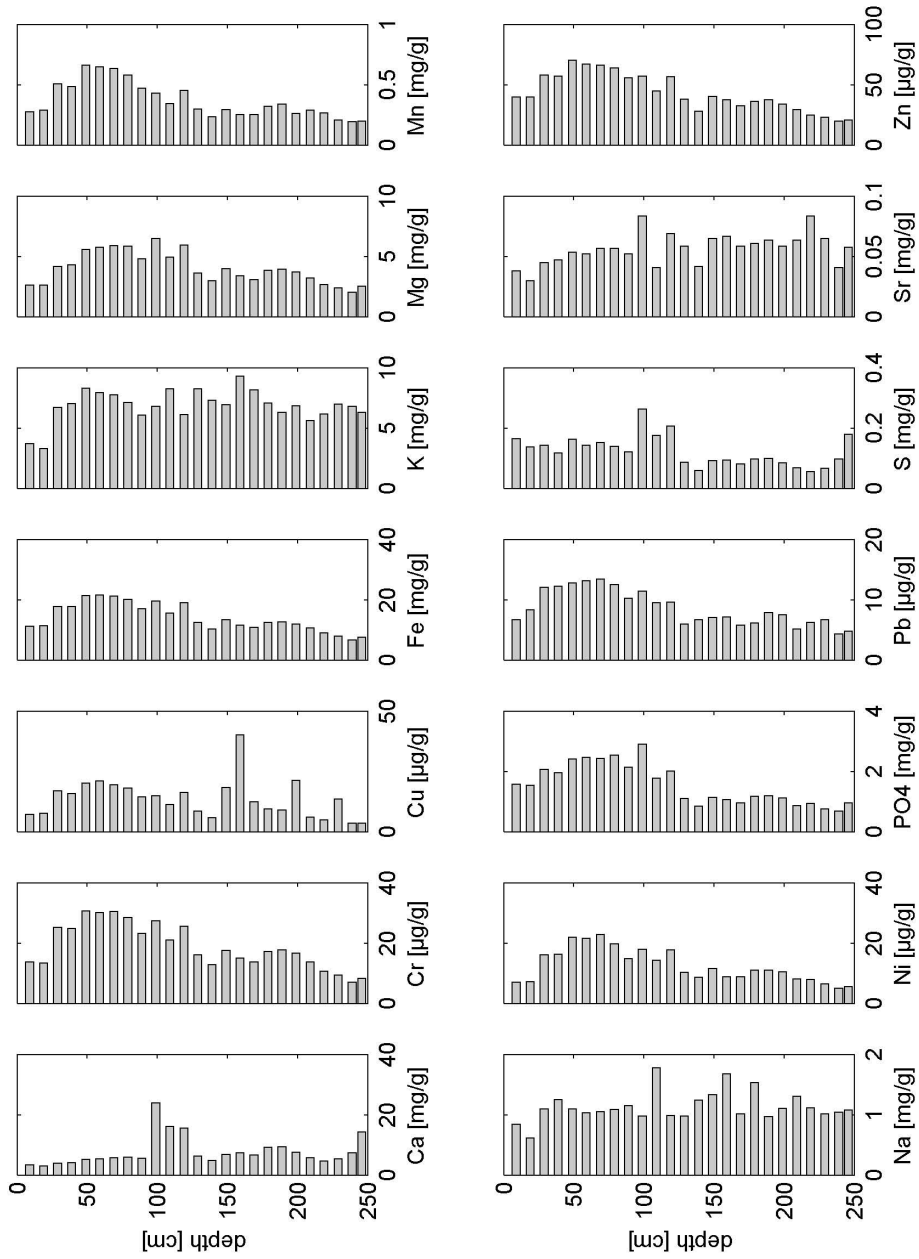

Fig. 4. Element composition of samples taken in study site 1.

Two VES were conducted in the vicinity of the outcrop (Fig. 2). VES #1A is located 10 m to the west of the outcrop and, thus, is assumed to reflect the outcrop structure. A four layer model was fit with an error of 2.753 and shows changes in resistivity in 1.5 and 2.3 m, from where a low-impedance layer with a apparent resistivity of 22 Ωm until a depth of 53 m is recognized (Fig. 5, #1A). VES #1B is located on a slope adjacent to the outcrop and reflects a shallow weathered layer. Generally higher resistivities are found throughout the profile and with a distinct increase at a depth of 10–11 m below surface (Fig. 5, #1B).

5.2 *Study site 2*

Study site 2 is located in a valley tributary to a major Ugii Nuur inflow in the northern part of the basin (Fig. 2). The cross section of the valley runs south-north and depicts a slightly inclined 1100 m wide saucer-shaped valley (Fig. 7). While the north-facing slope has a concave profile curvature, the south exposed slope features several knicks between rather straight slope sections. Although not well resolved by the DGPS measurements, the valley bottom exhibits a small V-shaped drainageway of approximately 3 m width and 1 m depth.

The substrata of the northward exposed slope transforms from schistous bedrock partially covered by blocky debris with a silty to sandy matrix at the hilltop. At the valley bottom we found silty sand with sparse occurrence of boulders and gravel. The south facing slope experiences a more distinct change in substrata from the valley bottom to the top. Alluvial cones build up by coarse gravel located at the hillslope base are attached to straight slope sections of exposed bedrock partly covered by boulders and debris. The slope is intermitted by a terrace-like flattening covered by few decimeters of debris and sand. Due to the lack of outcrops in this study site VES are the only information on the structure of the underground.

Fig. 7 shows the locations of VES. The electrode array of the Schlummberger configuration was expanded perpendicular to the cross valley profile to a maximum half current electrode spacing (s/2) of 100 m. The apparent resistivity versus electrode separation curves were modeled using three to six layer models with fitting errors ranging from 1.432 to 4.986. Insertion of multiple layers in the uppermost meter of the profile hereby yielded satisfying curve fitting in greater depths.

Relatively low variability in apparent resistivity ranging from 300 to 800 Ωm accounts for VES #2A and #2B that were surveyed on the northward exposed slope (Fig. 6). An increase in apparent resistivity at an electrode distance of 74 m suggests a layer with decreased conductivity in 40 and 55 m depth, respectively.

VES #2C and #2D are characterized by a more variable apparent resistivity-depth relationship. A strong decrease in apparent electrical resistivity occurs in depths between 8 and 9 m below surface and suggests a layer with higher electrical conductivity until a depth of about 21 to 27 m. A layer with a sharp increase in resistivity is recognized beneath. VES #2E and #2F show a less distinct highly conductive layer than VES #2C and #2E, but are also characterized by a sharp increase in resistivity in depths in 28 and 9 m below surface, respectively.

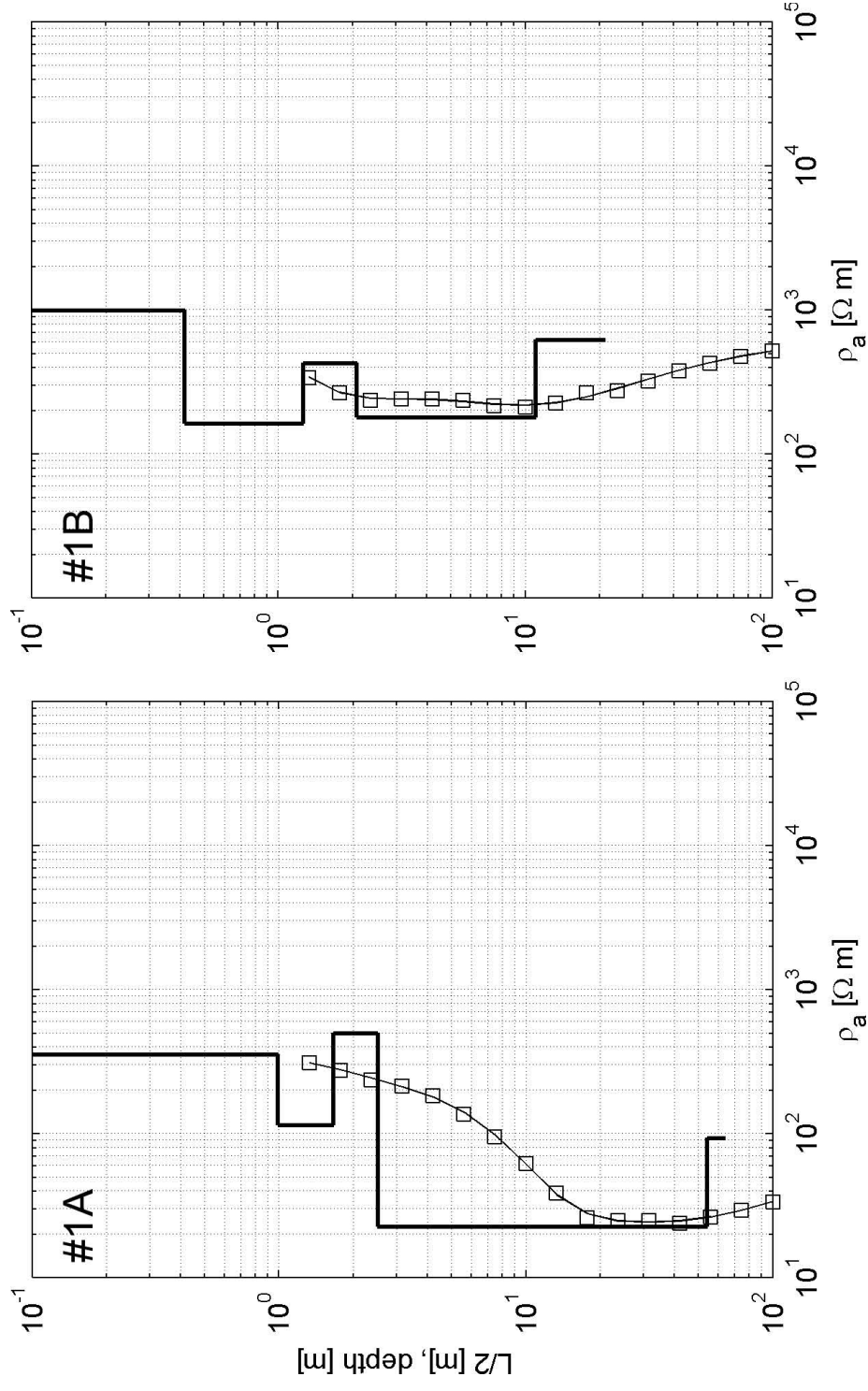

Fig. 5. One-dimensional electrical resistivity sounding profiles in study site 1.

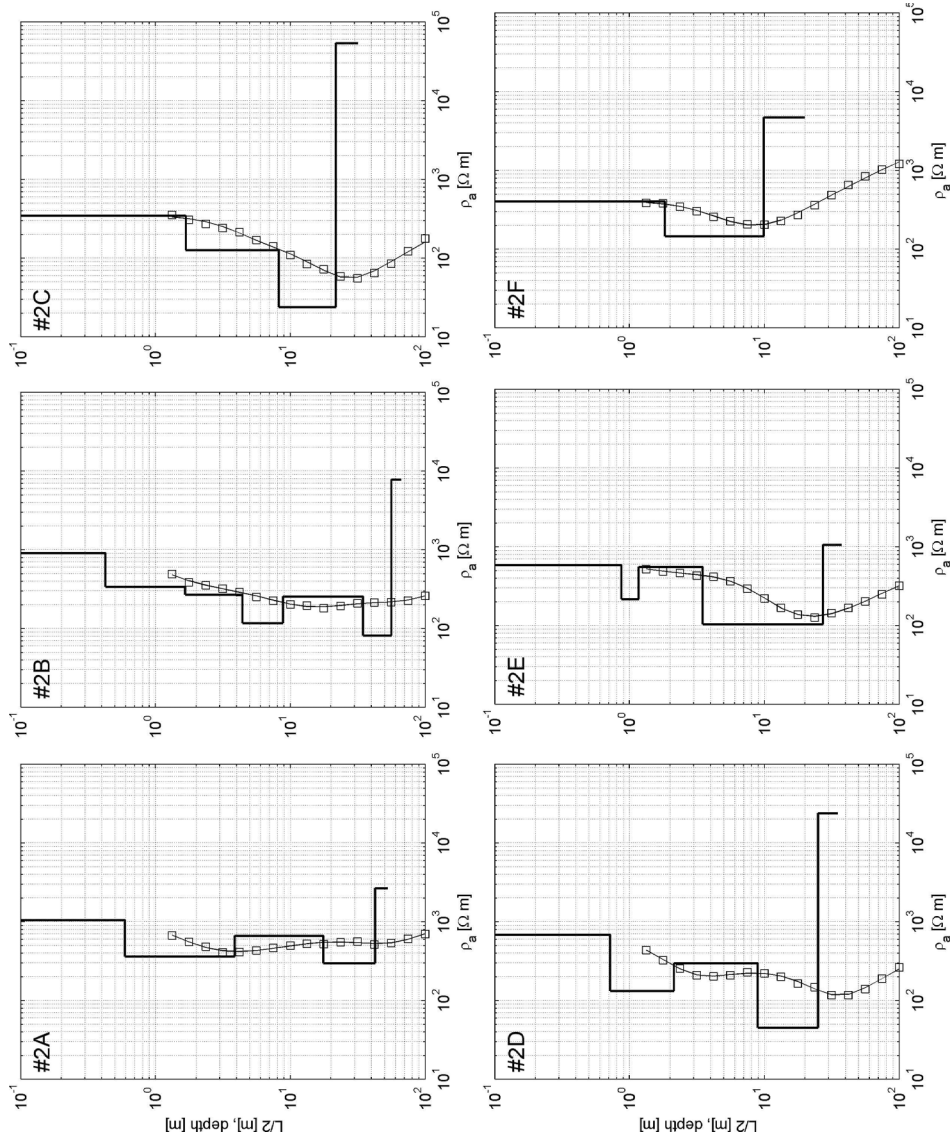

Fig. 6. One-dimensional electrical resistivity sounding profiles in study site 2.

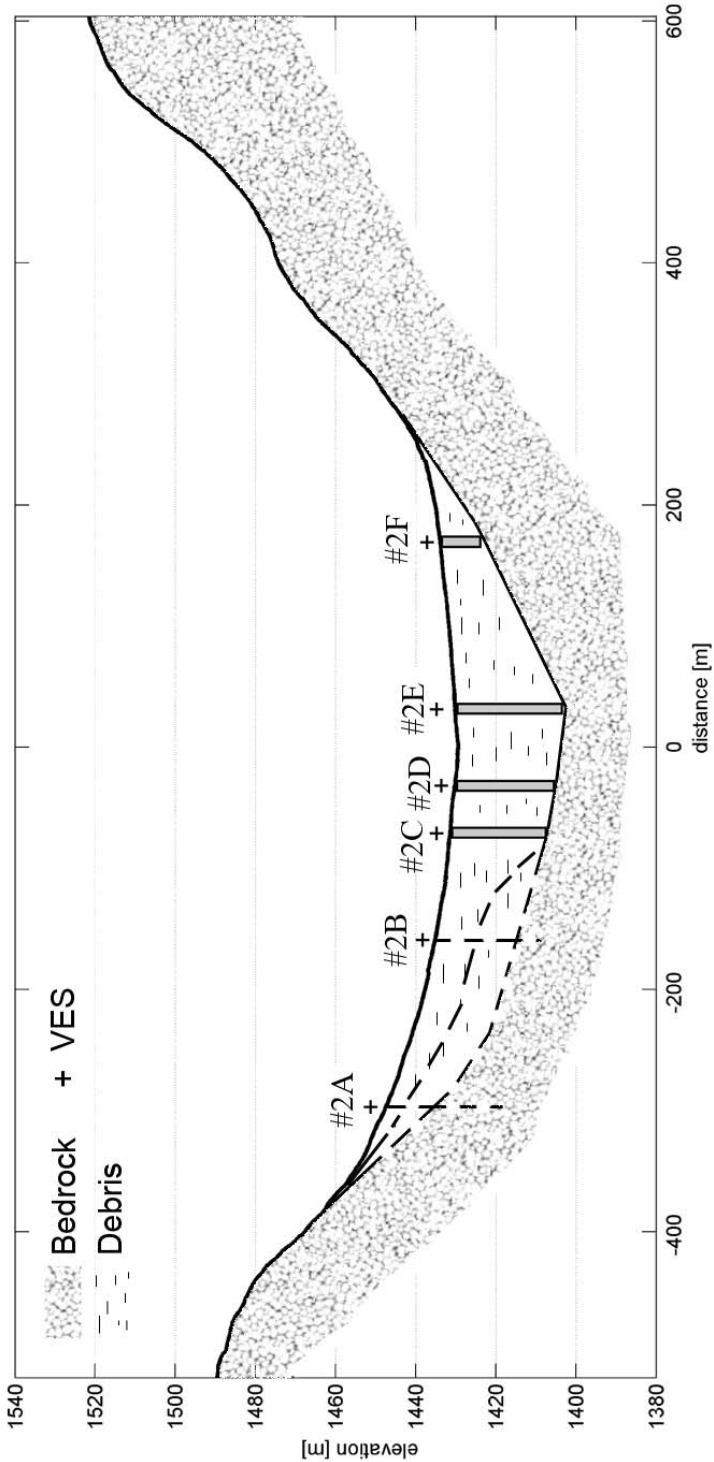

Fig. 7. Cross valley profile (direction: south to north), locations of one-dimensional vertical electrical soundings (VES) and interpreted subsurface relief in study site 2. Dashed lines refer to subsurface relief where VES yielded information too fuzzy to be interpreted adequate.

6 *Discussion*

6.1 *Study Site 1*

A timeframe of the profile in study site 1 was established by C dates derived from humins and humic acids. The dates can be interpreted as minimum age of a deposit if (1) organic material is deposited together with inorganic material or (2) strong evidence for synsedimentary, autochthonous pedogenic origin of the material is given. Introduction and exchange of new and old carbon (in situ production by roots, vertical movement by water and bioturbation) and the loss by microbial decomposition lead to high uncertainty in soil datings (Wang et al. 1996, Madsen et al. 1998, Birkeland 1999). Yet, this problem is assumed to be less important in arid and semiarid environments (Wang et al. 1996). Pessenda et al. (2001) show that datings of the humin fraction compared to charcoal datings generates reliable results in arid environments. Moreover, the carbonatic, cemented layer may constrict the vertical carbon exchange since it impairs bioturbation and percolation (Maki et al. 2007) and derogate the error of the determined ages. These arguments let us assume that the determined ages are reliable.

The prevalence of fine sand along the profile suggests the deposition of fines by aeolian processes (Pye 1995). Relatively homogeneous beds of fines and the presence of an adjacent dune field in the vicinity of the site (Fig. 2) support this hypothesis. Moreover, the higher fraction of silt in the upper 90 cm hints at two different phases of aeolian accumulation. While the lower part reflects low distance transport by saltation and reptation and hints at the occurrence of local or regional sand sources, the upper part of the profile points at a mixture of local redeposition and mineral dust deposition. Both types of aeolian deposits in steppe areas have been highlighted by Grunert & Lehmkuhl (2004) and Dill et al. (2006).

According to the datings, the boundary between these two phases is at the Early to Mid Holocene. Dryer conditions during the Late Pleistocene to Early Holocene are found in various areas in Mongolia, but differ from findings obtained in northern and western Mongolia (Prokopenko et al. 2007, Gunin et al. 1999). Such disagreements may be explained by local effects of melting water from glaciers (Walther 1999, Walther et al. 2003), but may also result from regionally varying influence of temperature on vegetation growth (Gunin et al. 1999). Yet, it has been inferred from lake sediments from Ugii Nuur by Schwanghart et al. (2008) that there is a change towards wetter conditions in the catchment at $\sim$8 ky BP. Pollen analysis by Rösch et al. (2005) on the same core provide evidence for a denser vegetation cover during this time. Hence, we suggest that the development of a denser vegetation cover during the Early to Mid Holocene both hampered sand mobilization and favored trapping of mineral dust. Long distance transport from the Gobi desert may serve as an explanation for the origins of the silt size particles. Yet, the importance of river and lake deposits has been highlighted by Grunert & Lehmkuhl (2004) and the sedimentary dynamics of the adjacent, highly meandering Orkhon River may serve as an explanation for the origin of the dust, too.

The origin of the carbonatic layer is likely connected to the aeolian accumulation of dust. Bedrocks in the area are poor in carbonates. Aeolian, calcareous and Ca-bearing deposits have been shown to play a major role in the generation of calcretes (Blümel 1981, Besler 1992, Birkeland 1999). Hence, a horizontal cycle of aeolian sediment redistribution as shown by Grunert & Lehmkuhl (2004) for western Mongolia might also apply in the Ugii Nuur basin. After deposition,

percolation and mobility in the soil profile led to the development of the carbonatic layer that is classified as a pedogenic calcrete in the first or second state of carbonate accumulation (Wright & Tucker 1991, Birkeland 1999). This is supported by findings of carbonate coatings on the bottom side of rock fragments throughout the catchment and other parts of Mongolia (Klinge 2001).

More favorable moisture conditions since Early to Mid Holocene can also be inferred from soil formation processes evidenced by the TOC and LOI profile (Fig. 3). While TOC contents usually tend to rapidly decrease with depth (Vallentyne 1962, Jobbágy & Jackson 2000, Maki et al. 2007) relatively constant values are found until a depth of 1 m. This distribution partly reflects the capacity of the finer texture in the first meter to hold organic matter (Scheffer & Schachtschabel 2002). Deep rooting and bioturbation also leads to organic carbon enrichment in greater depth (Jobbágy & Jackson 2000). Yet, high sedimentation rates caused by aeolian deposition or by soil erosion processes (Pickup & Chewings 1988, Hill & Schütt 2000) can also reduce oxygen availability in the soil and, thus impede microbial organic carbon decay (Lerman 1979). Moreover, positive correlation of TOC and (heavy) metal concentrations indicates metal-organic complexes (Moore 1973). They develop during phases of increased humidity when soil water causes locally a reducing environment and thus allows reduction, mobilization and successive bonding in metal-organic complexes (Moore 1973, Heikinnen 1990). In contrast, during arid conditions prevailing oxidising conditions cause immobility of mineral iron-bondings in soils (Krauskopf 1967, Mathess & Pekdeger 1980). As a consequence, we interpret the vertical distribution of TOC as an indicator for soil formation in combination with high sedimentation rates of aeolian and hillwash processes.

The findings in the sediment profile cannot be inferred from VES #1A. This is in contrast to findings of Baines et al. (2002) who show the applicability of electrical resistivity methods in mapping sand and gravel deposits buried by silt and clay. Obviously, the differences in electrical properties of the shallow subsurface are too small to discriminate different lithologies. Instead, lithological signals are likely to be superimposed by the higher amount of pore water that leads to a reduction of apparent resistivity in greater depths. Values around 20 to 30 Ωm indicate the presence of water with a relatively high ionic conductivity that arises from the presence of dissolved salts (Mussett & Khan 2000). An increase in apparent resistivity at 50–60 m depth can be interpreted as the boundary between the unconsolidated debris and consolidated bedrock as bedrock generally has a higher electrical resistivity than debris cover as long as the bedrock does not bare any ores (Mussett & Khan 2000). The deepest layer, however, is only based on a few resistivity values and thus may significantly vary in depth. VES #1B exhibits higher apparent resistivities throughout the profile. Due to a lack of a directly attached borehole or profile information interpretation of VES #1B can not be validated by field evidence. However, the persistent high resistivity values in the top ten meters is interpreted as a combination of sandy to blocky debris and consolidated, but weathered bedrock which is due to its position on the slope rather dry. An increase in resistivity at 10 m depth is interpreted to be the transition to the fresh, unweathered bedrock (Dahlin 2001).

6.2 *Study site 2*

Findings from VES surveyed at study site 2 could not be validated in the field. Here, however, especially VES #2C–F are rather distinct due to stronger contrasts in apparent resistivities. VES #2A and B show a similar behavior as VES #1B and represents the more diffuse character of slopes that might be substantially influenced by lateral variations in the underground and less distinct grain size distribution than in the valley bottoms. Interpretation of these VES in terms of layer thickness and composition are speculative and dashed lines in Fig. 7 account for the uncertainty in the deduction of subsurface relief. In the valley bottom strong increases in resistivity (VES #2C–F) have been recorded in 21–27 m below surface that most probably reflect the interface of debris covers and consolidated bedrock (Fig. 7).

7 *Conclusions*

We show that depositional environments in central Mongolia exhibit a far more complex genesis than the relatively uniform appearance of relief suggests. Since the Early to Mid Holocene input of mineral dust and fines plays a major role in the formation of the sedimentary architecture. This highlights the importance of long distance aeolian transport and probable sediment trapping by denser vegetation cover that reflects wetter conditions during this time in the Ugii Nuur basin. The existence of dust sources, however, suggests dryer conditions elsewhere. This impedes the transferability of these findings on wider areas. Subjacent substrata point at the higher importance of local sand mobilization and transport that suggest higher aridity during the Late Pleistocene and Early Holocene. Furthermore, it is demonstrated that electrical resistivity tomography is applicable to quantify thicknesses of the widespread debris accumulations found. The derivation of a subsurface relief suggests that valley fillings enrobe a strong bedrock relief.

Acknowledgements

Thanks to Dr. Henry Brasse (Freie Universität Berlin) for helpful discussion and assistance by interpreting 1D electrical resistivity tomography. Thanks to Prof. Dr. Dr. hc Michael Walther (National University of Mongolia) for valuable discussions, help during field work and logistics. Thanks to Tomasz Goslar (Poznan Radiocarbon Laboratory) assisting interpretation of C datings. Thanks to Dr. Röper for guidance and support in X-Ray diffraction analysis. Thanks to Altangerel Bat-Erdene, Judith Mahnkopf and Rikkardo Klinger and the participants of the International Field Class in 2005 and 2006 for assisting field work.

References

AG Bodenkunde (2005): Bodenkundliche Kartieranleitung. – Hannover, 5. ed.

Aspinall, A. & Gaffney, C.F. (2001): The Schlumberger array – potential and pitfalls in archaeological prospection. – Archaeol. Prosp. **8:** 199–209.

Baines, D., Smith, D.G., Froese, D.G., Bauman, P. & Nimeck, G. (2002): Electrical resistivity ground imaging (ERGI): a new tool for mapping the lithology and geometry of channel-belts and valley-fills. – Sedimentology **49:** 441–449.

Barthel, H. (1983): Die regionale und jahreszeitliche Differenzierung des Klimas in der Mongolischen Volksrepublik. – In: Barthel, H., Brunner, H., Haase, G. (eds.): Physisch-Geographische Studien in Asien. – BRNO, Stud. Geogr. **34:** 3–91.

Berkey, C.P. & Morris, K.K. (1927): Geology of Mongolia. – Amer. Mus. Natur. Hist., New York.

Besler, H. (1992): Geomorphologie der ariden Gebiete. – Erträge der Forschung **280**, Wissenschaftliche Buchgesellschaft, Darmstadt.

Birkeland, P.W. (1999): Soils and geomorphology. – Oxford Univ. Press, New York, Oxford, 3 ed.

Blümel, W.D. (1981): Pedologische und geomorphologische Aspekte der Kalkkrustenbildung in Südwestafrika und Südostspanien. – Karlsruher Geogr. Hefte **10**, Karlsruhe.

Bush, A.B. (2005): CO_2/H_2O and orbitally driven climate variability over central Asia through the Holocene. – Quatern. Int. **136:** 15–23.

Dahlin, T. (2001): The development of DC resistivity imaging techniques. – Comput. and Geosci. **27:** 1019–1029.

Dill, H.G., Khishigsuren, S., Majigsuren, Y., Myagmarsuren, S. & Bulgamaa, J. (2006): Geomorphological studies along a transect from the taiga to the desert in Central Mongolia – evolution of landforms in the mid-latitude continental interior as a function of climate and vegetation. – J. Asian Earth Sci. **27:** 241–264.

Dulam, J. (2005): Discriminate Analysis for Dust Storm Prediction in the Gobi and Steppe Regions in Mongolia. – Water, Air, Soil Pollution **5:** 37–49.

Fowell, S.J., Hansen, B.C., Peck, J.A., Khosbayar, P. & Ganbold, E. (2003): Mid to late Holocene climate evolution of the Lake Telmen basin, north central Mongolia, based on palynological data. – Quatern. Res. **59:** 353–363.

Grunert, J. & Dasch, D. (2004): Dynamics and evolution of dune fields on the northern rim of the Gobi Desert (Mongolia). – Z. Geomorph. N.F., Suppl. **133:** 81–106.

Grunert, J. & Lehmkuhl, F. (2004): Aeolian sedimentation in arid and semi-arid environments of Western Mongolia. – In: Smykatz-Kloss, W., Felix-Henningsen, P. (eds.): Paleoecology of Quaternary Drylands. – Springer, Berlin, New York, Toronto, Lecture Notes in Earth Sci. **102**, pp. 195–218.

Grunert, J., Lehmkuhl, F. & Walther, M. (2000): Paleoclimatic evolution of the Uvs Nuur basin and adjacent areas (Western Mongolia). – Quatern. Int. **65-66:** 171–192.

Gunin, P.D., Vostokova, E.A., Dorofeyuk, N.I., Tarasov, P.E. & Black, C.C. (1999): Vegetation dynamics of Mongolia. – Vol. **26** of Geobotany. Kluwer, Dordrecht, Boston, London.

Haase, G. (1983): Beiträge zur Bodengeographie der Mongolischen Volksrepublik. – In: Barthel, H., Brunner, H., Haase, G. (eds.): Physisch-Geographische Studien in Asien. – BRNO, Stud. Geogr. **34:** 231–367.

Hauck, C. & Vonder Mühll, D. (2003): Evaluation of geophysical techniques for application in mountain permafrost studies. – Z. Geomorph. N.F., Suppl. **132:** 161–190.

Heikinnen, K. (1990): Seasonal changes in iron transport and nature of dissolved organic matter in a humic river in Northern Finland. – Earth Surf. Processes and Landforms **15:** 583–596.

Herzschuh, U. (2006): Palaeo-moisture evolution in monsoonal Central Asia during the last 50,000 years. – Quatern. Sci. Rev. **25:** 163–178.

Hilbig, W. (1995): The vegetation of Mongolia. – SPB Academic Publishing, Amsterdam.

Hill, J. & Schütt, B. (2000): The use of remote sensing satellites for mapping complex patterns of erosion and stability in arid mediterranean ecosystems. – Remote Sensing Environ. **74:** 557–569.

Jadambaa, N., Grimmelmann, W. & Kampe, A. (2003): Hydrogeological map of Mongolia 1:1,000,000. Explanatory Notes. – Geol. Jb. **C69:** 3–50.

Jobbágy, E.G. & Jackson, R.B. (2000): The vertical distribution of soil organic carbon and its relation to climate and vegetation. – Ecol. Appl. **10:** 423–436.

Klinge, M. (2001): Glazialgeomorphologische Untersuchungen im Mongolischen Altai als Beitrag zur jungquartären Landschafts- und Klimageschichte der Westmongolei. – Aachener Geogr. Arb. **35**, Geographisches Institut der RWTH Aachen im Selbstverlag, Aachen.

Kneisel, C. (2003): Electrical resistivity tomography as a tool for geomorphological investigations – some case studies. – Z. Geomorph. N.F., Suppl. **132:** 37–49.

Kneisel, C. (2004): New insights into mountain permafrost occurrence and characteristics in glacier forefields at high altitude through the application of 2D resistivity imaging. – Permafrost and Periglacial Processes **15:** 221–227.

Kneisel, C. (2005): Detecting mountain permafrost and hazard assessment for debris flows through the application of electrical resistivity tomography – an example from the Swiss Alps. – Z. Geomorph. N.F., Suppl. **138:** 1–10.

Kottek, M., Grieser, J., Beck, C., Rudolf, B. & Rubel, F. (2006): World map of the Köppen-Geiger climate classification updated. – Meteorol. Z. **15:** 259–263.

Krauskopf, K.B. (1967): Introduction to Geochemistry. – McGraw-Hill, New York.

Krautblatter, M. & Hauck, C. (2007): Electrical resistivity tomography monitoring of permafrost in solid rock walls. – J. Geophys. Res. **112:** F02S20.

Lehmkuhl, F. & Haselein, F. (2000): Quaternary palaeoenvironmental change on the Tibetan Plateau and adjacent areas (Western China and Mongolia). – Quatern. Int. **65/66:** 121–145.

Lehmkuhl, F. & Lang, A. (2001): Geomorphological investigations and luminescence dating in the southern part of the Khangay and the Valley of the Gobi Lakes (Central Mongolia). – J. Quatern. Sci. **16** (1): 69–87.

Lerman, A. (1979): Geochemical processes, water and sediment environment. – John Wiley and Sons, Chichester, New York.

Löwner, M.O., Preston, N.J. & Dikau, R. (2005): Reconstruction of a colluvial body using geoelectrical resistivity. – Z. Geomorph. N.F. **49:** 225–238.

Madsen, D.B., Jingzen, L., Elston, R.G., Cheng, X., Bettinger, R.L., Kan, G., Brantingham, P.J. & Kan, Z. (1998): The loess/paleosol record and the nature of the younger dryas climate in Central China. – Geoarchaeol.: Intern. J. **13:** 847–869.

Maki, A., Kenji, T., Kiyokazu, K. & Teruo, H. (2007): Morphological and physico-chemical characteristics of soils in a steppe region of the Kherlen River basin, Mongolia. – J. Hydrol. **333:** 100–108.

Mathess, A. & Pekdeger, A. (1980): Chemisch-biochemische Umsetzungen bei der Grundwasserneubildung. – Gas- und Wasserfach **121:** 214–219.

Moore, T.R. (1973): The distribution of iron, manganese and aluminium in some soils from north-east Scotland. – J. Soil Sci. **24:** 162–171.

Mussett, A.E. & Khan, M.A. (2000): Looking into the earth. An introduction to geological geophysics. – Cambridge Univ. Press, Cambridge.

Natsagdorj, L., Jugder, D. & Chung, Y.S. (2003): Analysis of dust storms observed in Mongolia during 1937–1999. – Atmos. Environ. **37:** 1401–1411.

Opp, C. & Hilbig, W. (2003): Verbreitungsregeln von Böden und Pflanzengesellschaften im nördlichen Zentralasien unter besonderer Berücksichtigung des Uvs-Nuur-Beckens. – Petermanns Geogr. Mitt. **147:** 16–23.

Owen, L.A., Richards, B., Rhodes, E.J., Cunningham, W.D., Windley, B.F., Badamgarav, J. & Dorjnamjaa, D. (1998): Relic permafrost structures in the Gobi of Mongolia: age and significance. – J. Quatern. Sci. **13:** 539–547.

Owen, L.A., Windley, B.F., Cunningham, W.D., Badamgarav, J. & Dorjnamjaa, D. (1997): Quaternary alluvial fans in the Gobi of southern Mongolia: evidence for neotectonics and climate change. – J. Quatern. Sci. **12:** 239–252.

Peck, J.A., Khosbayar, P., Fowell, S.J., Pearce, R.B., Ariunbileg, S., Hansen, B.C. & Soninkhishig, N. (2002): Mid to Late Holocene climate change in north central Mongolia as recorded in the sediments of Lake Telmen. – Palaeogeogr., Palaeoclimat., Palaeoecol. **183:** 135–153.

Pessenda, L.C.R., Gouveia, S.E.M. & Aravena, R. (2001): Radiocarbon dating of total soil organic matter and humin fraction and its comparison with 14C ages of fossil charcoal. – Radiocarbon **43** (2B): 595–601.

Pickup, G. & Chewings, V.H. (1988): Forecasting patterns of erosion in arid land forms from Landsat MSS data. – Int. J. Remote Sensing **9:** 69–84.

Piro, S., Mauriello, P. & Cammarano, F. (2000): Quantitative integration of geophysical methods for archaeological prospection. – Archaeol. Prospection **7:** 203–213.

Prokopenko, A.A., Khursevich, G.K., Bezrukova, E.V., Kuzmin, M.I., Boes, X., Williams, D.F., Fedenya, S.A., Kulagina, N.V., Letunova, P.P. & Abzaeva, A.A. (2007): Paleoenvironmental proxy records from Lake Hovsgol, Mongolia, and a synthesis of Holocene climate change in the Lake Baikal watershed. – Quatern. Res. **68:** 2–17.

Pye, K. (1995): The nature, origin and accumulation of loess. – Quatern. Sci. Rev. **14:** 653–667.

Richter, H., Haase, G. & Barthel, H. (1963): Die Bildung von Gebirgsfußflächen im Gobi-Altai. – In: Harig, G. & Steinmets, M. (eds.): Lehre – Forschung – Praxis. – Die Karl-Marx-Universität zum zehnten Jahrestag ihrer Namensgebung am 5. Mai: pp. 198–213.

Rösch, M., Fischer, E., Märkle, T. (2005): Human diet and land use in the time of the Khans. – Archaeobotanical research in the capital of the Mongolian Empire, Qara Qorum, Mongolia. – Veget. Hist. and Archaeobot. **14:** 485–492.

Scheffer, F. (2002): Lehrbuch der Bodenkunde / Scheffer/Schachtschabel. – Spektrum, Heidelberg, Berlin, 15 ed.

Schwanghart, W., Schütt, B. & Walther, M. (2008): Holocene climate evolution of the Ugii Nuur basin, Mongolia. – Advanc. Atmos. Sci., MAIRS special issue, accepted.

Sirocko, F., Sarntheim, M., Erlenkeuser, H., Lange, H., Arnold, M. & Duplessy, J.C. (1993): Century-scale events in monsoonal climate over the past 24,000 years. – Nature **364**: 322–324.

Sladen, C. & Traynor, J.J. (2000): Lakes during the evolution of Mongolia. – In: Gierlowski-Kordesch, E.H. & Kelts, K.R. (eds.): Lake basins through space and time. – Amer. Assoc. Pet. Geol. Stud. in Geology **46:** 35–57.

Tarasov, P., Dorofeyuk, N. & Metel'Tseva, E. (2000): Holocene vegetation and climate changes in Hoton-Nur basin, northwest Mongolia. – Boreas **29:** 117–126.

Traynor, J.J. & Sladen, C. (1995): Tectonic and stratigraphic evolution of the Mongolian People's Republic and its influence on hydrocarbon geology and potential. – Marine and Pet. Geology **12:** 35–52.

Vallentyne, J.R. (1962): Solubility and the decomposition of organic matter in nature. – Arch. Hydrobiol. **58:** 423–434.

Walther, M. (1999): Befunde zur jungquartären Klimaentwicklung rekonstruiert am Beispiel der Seespiegelstände des Uvs Nuur-Beckens (NW-Mongolei). – Die Erde **130:** 131–150.

Walther, M. & Gegeensuvd, T. (2005): Ugii Nuur (Central Mongolia) paleo-environmental studies of lake level fluctuations and Holocene climate change. – Geograph. Oekol. **2**. MOLARE Research Centre, Ulaanbaatar.

Walther, M. & Naumann, S. (1997): Beobachtungen zur Fußflächenbildung im ariden bis semiariden Bereich der West- und Südmongolei (Nördliches Zentralasien). – Stuttgarter Geograph. Stud. **126:** 154–171.

Walther, M., Wünnemann, B. & Tschimeksaichan, A. (2003): Seen und Paläoseen in der Mongolei und Nordwestchina. – Petermanns Geograph. Mitt. **147** (5): 40–47.

Wang, L., Sarnthein, M., Erlenkeuser, H., Grimalt, J., Grootes, P., Heilig, S., Ivanova, E., Kienast, M., Pelejero, C. & Pflaumann, U. (1999): East Asian monsoon climate during the Late Pleistocene: high-resolution sediment records from the South China Sea. – Mar. Geol. **156:** 245–284.

Wang, Y., Amundson, R. & Trumbore, S. (1996): Radiocarbon dating of soil organic matter. – Quatern. Res. **45:** 282–288.

Watson, A. & Nash, D.J. (1997): Desert crusts and varnishes. – In: Thomas, D.S.G. (ed.): Arid zone geomorphology. – Process, form and change, Wiley, Chichester. 2 ed., pp. 70–107.

Wright, V.P. & Tucker, M.E. (1991): Calcretes. An introduction. – In: Wright, V.P. & Tucker, M.E. (eds.): Calcretes, Blackwell, Oxford, London. Repr. Ser. **2**, Int. Assoc. Sediment., pp. 1–22.

Yang, X., Rost, K.T., Lehmkuhl, F., Zhenda, Z. & Dodson, J. (2004): The evolution of dry lands in northern China and in the Republic of Mongolia since the Last Glacial Maximum. – Quatern. Int. **118-119:** 69–85.

Adresses of the authors:
Wolfgang Schwanghart, University of Basel, Department of Environmental Sciences, Physical Geography and Environmental Change, Klingelbergstr. 27, CH-4056 Basel. w.schwanghart@unibas.ch.
Prof. Brigitta Schütt, Institut für Geographische Wissenschaften, Freie Universität Berlin, Malteserstr. 74-100, 12249 Berlin.